Novel Wind Power Grid-connection System Using Inductive Filtering Technology*

Juan Ni[1], *Sijia Hu*[1*], *Yong Li*[1*], *Jinjie Lin*[1], *Qianyi Liu*[2], *Peiyao Liu*[1] *and Lihong Dong*[1]
(1. College of Electrical and Information Engineering, Hunan University, Changsha 410082, China;
2. School of Automation, Central South University, Changsha 410083, China)

Abstract: Herein, a novel wind power grid-connection system based on inductive filtering is proposed to improve grid-connection compatibility, and is implemented in a 50-MW real system. First, the topology and wiring configuration of the proposed system are discussed. Thereafter, an equivalent circuit and mathematical model are established to reveal the filtering characteristics and resonance damping mechanism of the proposed system. Finally, a 50-MW wind farm-based experimental study, which is conducted to validate the effectiveness and availability of the system is discussed. The experimental results show that the main harmonics, power factor, voltage fluctuation, and flicker satisfy national standards.

Keywords: Wind power generation, inductive filtering method, grid-connection compatibility, power quality

1 Introduction

In response to the intensifying global energy crisis, wind power has been developed rapidly in recent years [1]. However, with the increasing application of wind energy, associated grid connection problems have become prominent; hence, comprehensive management of the voltage, power quality (PQ), and stability of wind power systems is indispensable [2-5].

Harmonics distort waveforms, generate excessive losses, and their high-order components, introduced through power electronic devices, may trigger resonance under certain conditions, resulting in harmonic amplification, serious harmonic pollution, and a weak safety state of the grid-connected system [6]. Reactive power is a key factor in wind farms. The lack of adequate dynamic reactive power tends to aggravate dynamic voltage security in large-scale wind-integrated power systems, particularly near the point of common coupling (PCC) [7].

Traditionally, wind farms have adopted passive power filters (PPFs) or active power filters (APFs) for harmonic suppression [8]. However, the filtering performance of the PPF is susceptible to disturbances from both the external system and the design parameters [9]. Although APFs have a better filtering performance compared with PPFs, these power filters are limited by the complexity of the control system and the cost in high-power applications. The inductive filtering method introduced in Refs. [10-13] has been proven as a more suitable choice because it can automatically "induct" reverse harmonic currents via the construction of a transformer whose equivalent impedance of the filtering winding is 0, and its outside is connected to properly design passive filtering branches. Hence, theoretically, there is no harmonic in the grid-side winding. It can be expected that adopting the inductive filtering method in wind power grid-connection system applications will improve the performance; however, no real application example has been reported.

In most cases, voltage and reactive power control can be achieved using capacitor banks, static var compensators (SVCs), and static var generators (SVGs) [14]. In Ref. [15], capacitor and reactor banks were used to maintain the voltage and power factor according to the commands of an integrated control system; however, the response was not sufficiently fast.

Manuscript received June 15, 2021; revised August 25, 2021; accepted September 25, 2021. Date of publication September 30, 2022; date of current version May 6, 2022.
* Corresponding Author, E-mail: huda_hsj@163.com, yongli@hnu.edu.cn
* Supported by the International Science and Technology Cooperation Program of China (2018YFE0125300), the Fundamental Research Funds for the Central Universities (531118010661), the National Natural Science Foundation of China (52061130217), the Innovative Construction Program of Hunan Province of China (2019RS1016), the 111 Project of China (B17016), and the Excellent Innovation Youth Program of Changsha of China (KQ2009037).
Digital Object Identifier: 10.23919/CJEE.2022.000029

SVCs use thyristor-regulated reactance plus multigroup capacitors to realize reactive power control; however, resonance may be caused in practice [16] because an SVC reforms the structure and parameters of the system. The authors of Ref. [17] verified that under different disturbances, such as wind speed changes or short-circuit faults, a power oscillation damping controller-embedded SVG can improve the stability of a two-area power system connected to onshore and offshore wind farms. In addition, compared with SVCs, SVGs have a faster response, better compensation performance, lower harmonic interference level, and smaller energy storage component size. Therefore, SVGs are preferred in modern systems to improve the voltage stability and meet the reactive power demand at the grid-connection point.

Considering the real application in this study, a novel and successful wind power grid-connection system based on the inductive filtering method is proposed herein for harmonic, resonance, reactive power, and voltage management. The proposed system comprises an inductive filtering transformer (IFT), SVG, and two fully tuned passive filter (FTPF) branches. As will be discussed, the proposed system can significantly improve the operating performance and reliability of wind power systems with relatively high cost efficiency.

The remainder of this paper is organized as follows: Section 2 presents the topology, equivalent circuit, and mathematical model of the proposed system. Section 3 includes analyses of the filtering characteristics and resonance damping mechanism of the proposed system, besides some design notations. Next, verification via the 50-MW wind farm-based experiment is presented in Section 4. Finally, Section 5 concludes the study.

2 New wind power grid-connection system

2.1 Topology and system description

The topology of the proposed system is depicted in Fig. 1. As the connection point of utility, wind farm, and compensation devices, the IFT constitutes three specifically designed windings, i.e., W1, W2, and W3, which are grid-winding, load-winding, and filtering-winding, respectively. W1 and W2 are connected to the grid and the wind farm, respectively. Both the FTPFs and SVG are connected to W3 to form the superconducting induction principle-based inductive filtering condition [18], as well as dynamically regulate the reactive power and voltage of the PCC.

Combining the IFT and FTPFs can effectively suppress harmonics, reduce the risk of resonance, and improve the power factor; in this process, the harmonic flux and the related harmonic losses of the transformer can be reduced at a low level [19-20]. Meanwhile, the combination of the SVG and FTPFs, as a self-adjusted reactive power source, can improve the dynamic performance of the voltage at the PCC, while decreasing the capacity of the SVG, thus reducing the cost of the converter. The proposed system can improve the overall performance of wind power grid-connection systems, and hence was adopted in practice.

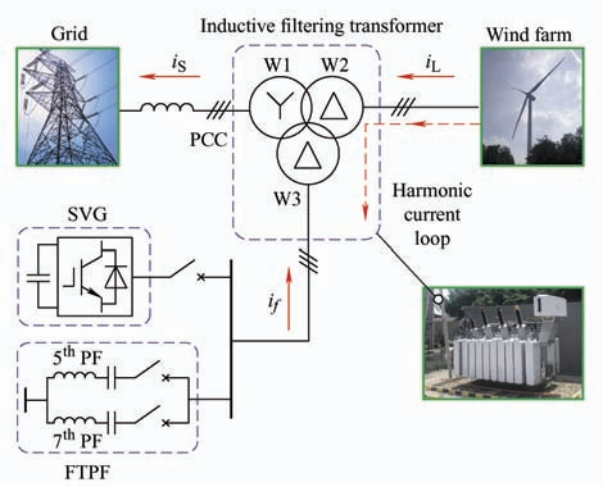

SVG: static var generator PCC: point of common coupling
PF: power filter FTPF: fully tuned passive filter

Fig. 1 Topology of the proposed system

The proposed system was applied to a real wind farm in Hunan Province, China. Fig. 2 shows the main electrical wiring diagram and on-site photos. The wind farm comprises 25 direct-driven permanent magnet synchronous generators (PMSGs), each with the rating of 2 MW (XE105-2000, XEMC), with a total installed capacity of 50 MW.

Each wind turbine (WT) connects to a 35 kV cable-based network via a 2.2 MV • A, 0.69 kV/35 kV step-up transformer, forming three groups: group 1: 1#-8# WTs, group 2: 9#-17# WTs, and group 3: 18#-25# WTs. These groups are connected to a

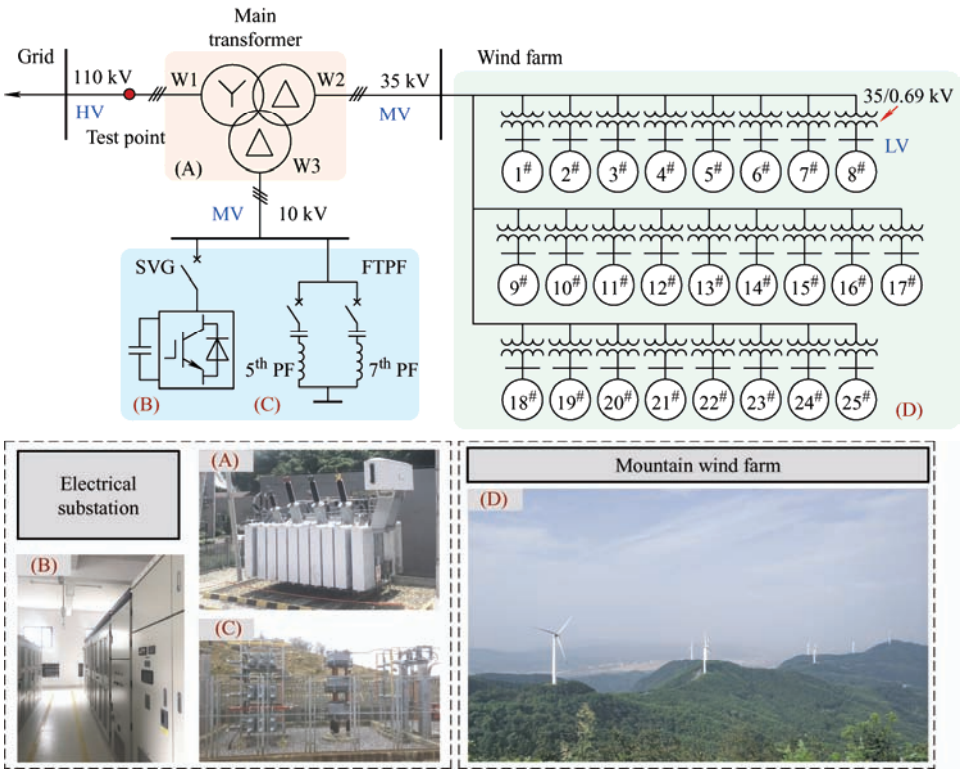

Fig. 2 Specifications of the proposed system used in a real wind farm

common 35-kV bus via cables and then pass through a YNd11+d11 main transformer (i.e., IFT) connected to a 110 kV public grid; the specifications of the IFT are provided in Tab. 1. The compensation devices, i.e., the FTPFs (5th and 7th harmonic filters) and a 6-Mvar SVG, connect to a 10 kV bus output from W3 of the IFT, and their specifications are listed in Tab. 2.

Tab. 1 Specifications of main transformer (IFT)

Parameter	Grid-winding(W1)	Load-winding(W2)	Filtering-winding(W3)
Rated voltage/kV	115	36.75	10.5
Rated capacity/(MV • A)	50	50	12
Short-circuit impedance(%)	Z_{k12}=11.01	Z_{k23}=4.33	Z_{k13}=7.03
No-load loss/(kV • A)		28.40	

Tab. 2 Specifications of passive filters

Item	5th filter	7th filter
Capacitance/μF	95.493	95.493
Inductance/mH	4.244	2.165
Total reactive power rating /Mvar	6	

2.2 Mathematical model of the proposed system

Fig. 3 presents the single-phase equivalent circuit model of the proposed system, where VSC-based WT generators can be regarded as the current source. As the SVG focuses on reactive power generation, its harmonic currents are negligible, such that the branch where the SVG is located can be regarded as an open circuit.

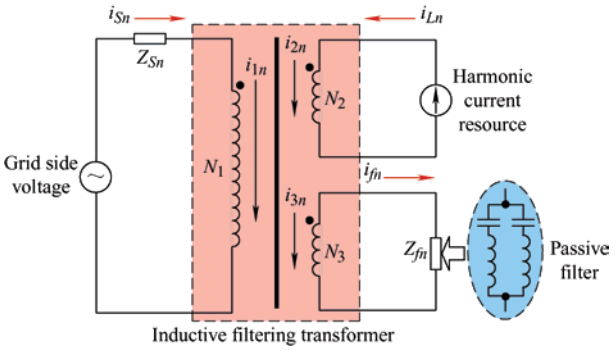

Fig. 3 Equivalent circuit of the proposed system (single-phase)

According to Fig. 3, the boundary condition at the n^{th} harmonic frequency can be expressed as

$$\begin{cases} U_{1n}=U_{Sn}-I_{Sn}Z_{Sn} \\ U_{3n}=I_{fn}Z_{fn} \end{cases} \tag{1}$$

$$\begin{cases} I_{Sn}=I_{1n} \\ I_{2n}=I_{Ln} \\ I_{3n}=-I_{fn} \end{cases} \tag{2}$$

where U_{1n}, U_{2n}, and U_{3n}, and I_{1n}, I_{2n}, and I_{3n} are the harmonic voltages and currents of W1, W2, and W3 of the IFT, respectively; I_{Sn}, I_{Ln}, and I_{fn} are the n^{th}-order harmonic currents at the grid side, load side, and filtering equipment side, respectively; Z_{Sn} is the system impedance of the grid; Z_{fn} is the equivalent impedance of the passive filters; and U_{Sn} is the background harmonic voltage.

According to the transformer magnetic potential balance principle and multi-winding transformer theory [21], the following basic equations of the IFT can be obtained

$$N_1 I_{1n}+N_2 I_{2n}+N_3 I_{3n}=0 \tag{3}$$

$$\begin{cases} U_{2n}-\dfrac{N_2}{N_1}U_{1n}=-\dfrac{N_1}{N_1}Z_{k21}I_{1n}-\dfrac{N_3}{N_2}Z_{2n}I_{3n} \\ U_{2n}-\dfrac{N_2}{N_3}U_{3n}=-\dfrac{N_3}{N_2}Z_{k23}I_{3n}-\dfrac{N_1}{N_2}Z_{2n}I_{1n} \end{cases} \tag{4}$$

where N_1, N_2, and N_3 represent the number of turns of W1-W3; and Z_{k21}, Z_{k23}, and Z_{k13} are the short-circuit impedances of W2 and W1, W2 and W3, and W1 and W3, respectively.

Z_{in} (i=1, 2, 3) is the equivalent impedance of Wi (i=1, 2, 3) of the IFT, and Z_i (i=1, 2, 3) can be easily calculated using Z_{k21}, Z_{k23}, and Z_{k13} [21] as follows

$$\begin{cases} Z_1=\dfrac{1}{2}\left(Z_{k21}+Z_{k13}-Z_{k23}\right) \\ Z_2=\dfrac{1}{2}\left(Z_{k21}+Z_{k23}-Z_{k13}\right) \\ Z_3=\dfrac{1}{2}\left(Z_{k31}+Z_{k23}-Z_{k12}\right) \end{cases} \tag{5}$$

Based on Eq. (5) and the parameters listed in Tab. 1, the values of Z_1, Z_2, and Z_3 in the fundamental frequency were calculated as 6.855%, 4.155%, and 0.175%, respectively.

Eqs. (1)-(5) form the basic mathematical model of the proposed system, from which the primary harmonic current I_{Sn} can be calculated using

$$I_{Sn}=\frac{N_3^2 U_{Sn}-N_1 N_2\left(Z_{3n}+Z_{fn}\right)I_{Ln}}{N_1^2\left(Z_{3n}+Z_{fn}\right)+N_3^2\left(Z_{1n}+Z_{Sn}\right)} \tag{6}$$

3 Operating mechanism analysis

Electric parameters may deviate from their original values in practice, which is regarded as a parameter disturbance and may cause performance degradation. It can be seen from Eq. (6) that the primary harmonic current I_{Sn} is influenced by two types of parameters: ① IFT internal parameters, including the equivalent impedances Z_{1n}, Z_{3n}, and Z_{fn} of W1, W3, and FTPF, respectively; and ② IFT external parameter: grid-side internal impedance Z_{Sn}.

To analyze the influence of the key parameters on the harmonic suppression and resonance damping performances of the proposed system, the sensitivities of the primary harmonic current to the load harmonic current and grid-side harmonic voltage of the IFT, that is, C_{i_IFT} and C_{v_IFT}, were defined as follows

$$\begin{cases} C_{i\_IFT}=\left|\dfrac{\partial I_{Sn}}{\partial I_{Ln}}\right|=\left|\dfrac{N_1 N_2\left(Z_{3n}+Z_{fn}\right)}{N_1^2\left(Z_{3n}+Z_{fn}\right)+N_3^2\left(Z_{1n}+Z_{Sn}\right)}\right| \\ C_{v\_IFT}=\left|\dfrac{\partial I_{Sn}}{\partial U_{Sn}}\right|=\left|\dfrac{N_3^2}{N_1^2\left(Z_{3n}+Z_{fn}\right)+N_3^2\left(Z_{1n}+Z_{Sn}\right)}\right| \end{cases} \tag{7}$$

From Eq. (7), C_{i_IFT} (or C_{v_IFT}) indicate that the primary harmonic current is induced by the per-unit load harmonic current (or grid-side harmonic voltage), so a low value of C_{i_IFT} or C_{v_IFT} indicates high harmonic/resonance suppression ability. Based on Eq. (7), and Tabs. 1 and 2, the filtering characteristics and resonance damping mechanism of the proposed system were analyzed. In this analysis, only reactance calculations were involved because the influence of resistance can be ignored in the concerned system.

The influences of X_{3n}+X_{fn} and X_{1n} on C_{i_IFT} and C_{v_IFT} in 250 Hz are plotted in Fig. 4 (note: in Fig. 4, $D_{(X3n+Xfn)}$ and D_{X1n} are the ratios of X_{3n}+X_{fn} and X_{1n} to their original design values, respectively; and L_S is fixed at its measured value of 25.7 mH). From Fig. 4a, if X_{3n} and X_{fn} are approximately equal to 0, C_{i_IFT} tends to 0, so the harmonic current generated by the wind farm can be counteracted by the magnetic flux by W3 through the quasi-superconducting induction of the loops of N_3 and X_{fn} in Fig. 3; this is the filtering mechanism of the IFT. However, Fig. 4b shows that as X_{3n}+X_{fn}→0, the risk of generating series resonance (SR) in the proposed system increases. In fact, if we appropriately increase X_{1n} in the designing stage of the IFT, as can be seen from Fig. 4b, the SR risk level decreases rapidly. Fortunately, C_{i_IFT} is insensitive to variations in X_{1n} (Fig. 4a), such that the suppressing ability of the harmonic current can be maintained

when X_{1n} increases. From the above discussion, it can be concluded that the proposed system has a good ability to block the harmonics generated from both grid harmonic voltage and load harmonic current.

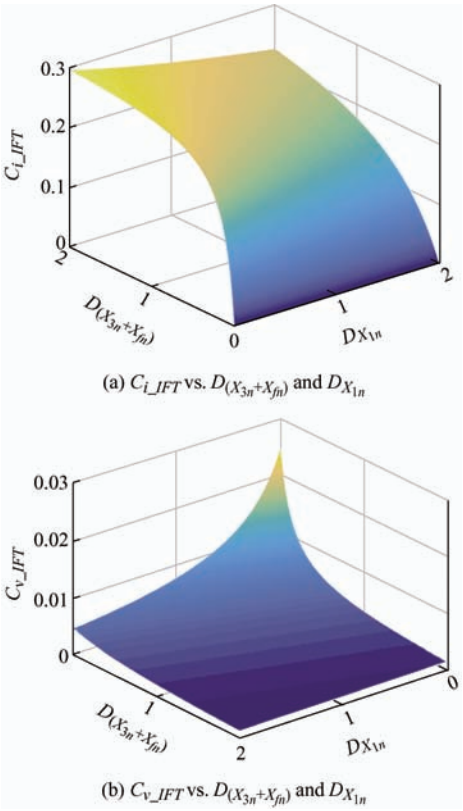

Fig. 4 Influences of key parameters on C_{i_IFT} and C_{v_IFT}

In practice, the 5th, 7th, 11th, and 13th harmonic currents are the dominant components in wind power grid-connection systems [22]. When a traditional filtering scheme was adopted for harmonic suppression, Ref. [23] indicates that the filtering performance was significantly affected by changes in the grid-side internal impedance. To evaluate the filtering performance of the proposed system considering variation in the grid-side internal impedance, the relationship between D_{Ls} and C_{v_IFT} is shown in Fig. 5 (note: D_{Ls} is the ratio of L_S to its measured value of 25.7 mH).

From Fig. 5, even if the value of the grid-side internal impedance changes over a wide range, the value of C_{v_IFT} remains less than 1.0%, implying that the filtering performance of the proposed system for the grid background harmonic voltage is slightly affected by L_S. From Fig. 5, we also find that C_{v_IFT} values in the 5th and 7th harmonic frequencies are larger than those in the 11th and 13th harmonic frequencies because the 5th and 7th passive filter branches supply two low-impedance paths for background harmonic voltages through the IFT. Moreover, the solid lines (X_1=6.8%) are all lower than the dotted lines (X_1=6.0%) in Fig. 5, indicating that the harmonic filtering capability of the proposed system can be improved by appropriately increasing the value of X_{1n} in its design stage, which is consistent with the analysis in Fig. 4.

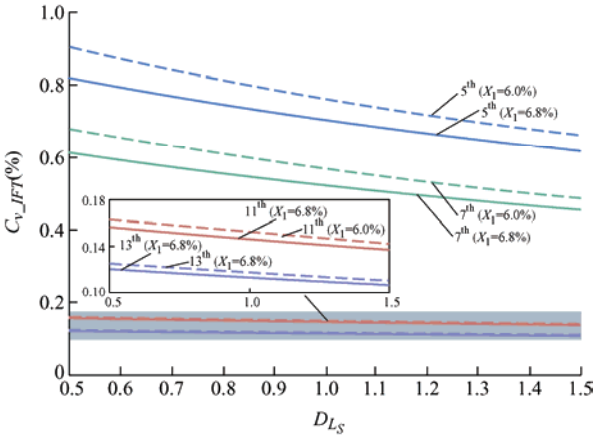

Fig. 5 Influence of L_S on C_{v_IFT} for varying X_1

The relationship between D_{Ls} and the primary harmonic current (induced by the load harmonic current) filtering rate, that is, 1-C_{i_IFT}, in the 5th, 7th, 11th, and 13th harmonic frequencies is displayed in Fig. 6. It can be seen that the filtering performance of the proposed system for load harmonic current is insensitive to the variation in L_S. In addition, the harmonic filtering rate of the proposed system under the 5th and 7th background harmonics is theoretically greater than 90.8%. Moreover, 34%-45% of the 11th and 13th harmonics from the load side can be suppressed, and this performance improves when L_S increases. To achieve a satisfactory filtering performance, the number of installed FTPF branches is determined by the harmonic amount and cost efficiency in practice. In our system, the 11th and 13th currents from the load side are not serious, so adopting the 5th and 7th FTPF branches, which can filter a small amount of the 11th and 13th currents, can satisfy the industrial demand.

The single-phase equivalent circuit of the traditional filtering method is depicted in Fig. 7, in which passive filter branches are installed on the WT side. Similar to the above analysis process, the expressions of the grid-side harmonic current I_{Sn2} and its sensitivities to the load harmonic current and grid-side harmonic

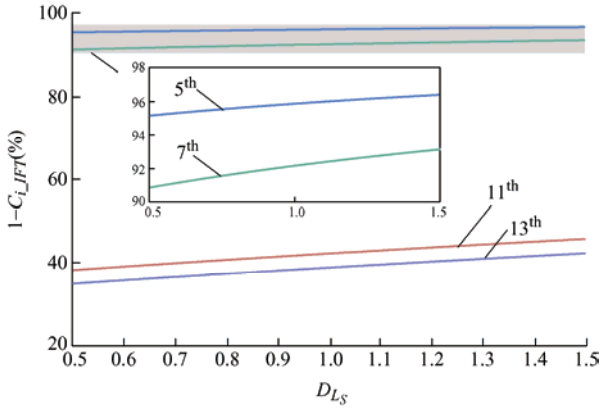

Fig. 6 Influence of L_S on 1-C_{i_IFT}

voltage, i.e., $C_{i\_Trad.}$ and $C_{v\_Trad.}$, can be obtained using Eqs. (8) and (9) as follows

$$I_{Sn2}=\frac{N_2^2U_{Sn}-N_1N_2Z_{fn}I_{Ln2}}{N_1^2Z_{fn}+N_2^2Z_{Sn}} \tag{8}$$

$$\begin{cases} C_{i\_Trad.}=\left|\dfrac{\partial I_{Sn2}}{\partial I_{Ln2}}\right|=\left|\dfrac{N_1N_2Z_{fn}}{N_1^2Z_{fn}+N_2^2Z_{Sn}}\right| \\ C_{v\_Trad.}=\left|\dfrac{\partial I_{Sn2}}{\partial U_{Sn}}\right|=\left|\dfrac{N_2^2}{N_1^2Z_{fn}+N_2^2Z_{Sn}}\right| \end{cases} \tag{9}$$

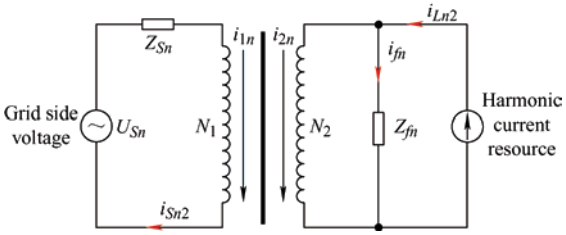

Fig. 7 Equivalent circuit of the traditional filtering system

To analyze the resonance damping performance, the relationship between the deviation of the inductance and capacitance of the 5th passive filtering branch and C_{i_IFT}, $C_{i\_Trad.}$, C_{v_IFT}, and $C_{v\_Trad.}$ at 250 Hz is provided in Fig. 8 (note: in Fig. 8, D_L^{5th} and D_C^{5th} are the ratios of the inductance and capacitor of the 5th passive filtering branch to their original design values (Tab. 2), respectively.

From Fig. 8, when the inductance and capacitor have values in the range of 0.9-1.1, resonance is easily triggered in the conventional system (see the darker peaks of $C_{i\_Trad.}$ and $C_{v\_Trad.}$ in Fig. 8); whereas, the peaks of C_{i_IFT} and C_{v_IFT} are outside this range. In addition, the amplitudes of the peaks of the proposed system in Fig. 8 are significantly lower than the conventional ones ($C_{i\_IFT\_peak}$=197.5, $C_{i\_Trad.\_peak}$=541.4, $C_{v\_IFT\_peak}$=81.9, $C_{v\_Trad.\_peak}$=198.2), indicating that the proposed IFT-based system is more robust against filter parameter disturbance compared with the conventional system.

Analysis and results of the relationship between C_{i_IFT}, $C_{i\_Trad.}$, C_{v_IFT}, $C_{v\_Trad.}$ and the L and C disturbances of the 7th passive filtering branch are similar to those in the above case. In practice, considering that the reactive power demand is low, sometimes, the 5th FTPF is the only filtering branch in operation, and sometimes, the 7th passive filtering branch; therefore, the above analysis of the 5th passive filter is representative and has its application background.

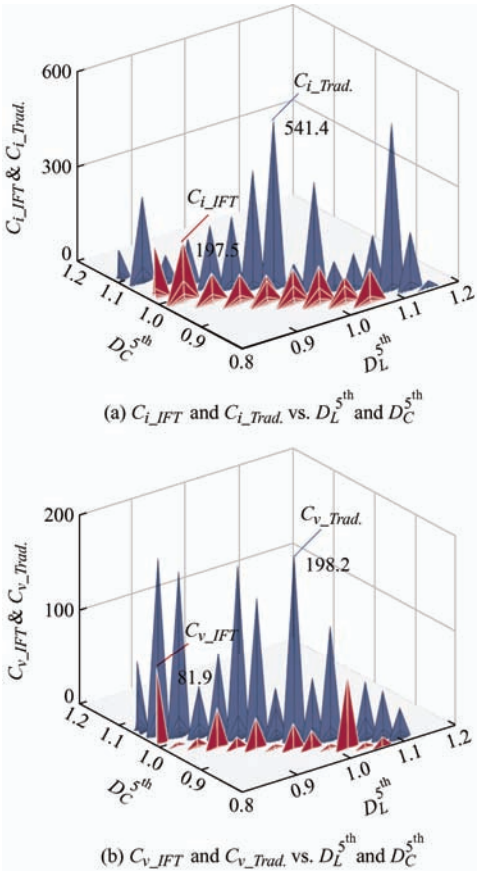

Fig. 8 Harmonic resonance damping performance under filter parameter disturbances

In the next section, experimental data from a real 50-MW IFT-based wind farm system, as depicted in Fig. 2, are used to verify the above analysis and conclusions.

4 Experimental verification

A HIOKI PW-3198 was installed at the 110-kV I-bus bar of the concerned wind farm to record data from 30 June to 29 July (~1 month) of 2020 with the sampling interval of 15 s for experimental verification, in which

PQ indicators such as harmonics, PF, voltage fluctuation, and flicker, were analyzed in detail (see the test point in Fig. 2).

4.1 Harmonics

Trend charts of several major harmonic current components and the total harmonic distortion of the public network voltage (THD_V) are shown in Fig. 9. Tabs. 3 and 4 present their respective specifications. From Tab. 4, all the 95% probability values of the concerned harmonic currents are lower than the limited values. Moreover, the values of THD_V (Tab. 3) are within the allowable level of the national standard (2%), which further proves the good harmonic-filtering performance of the proposed system.

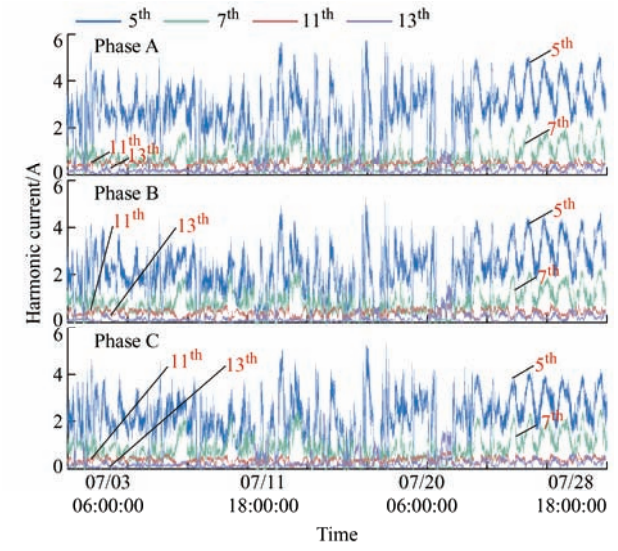

(a) Trend chart of harmonic currents at PCC

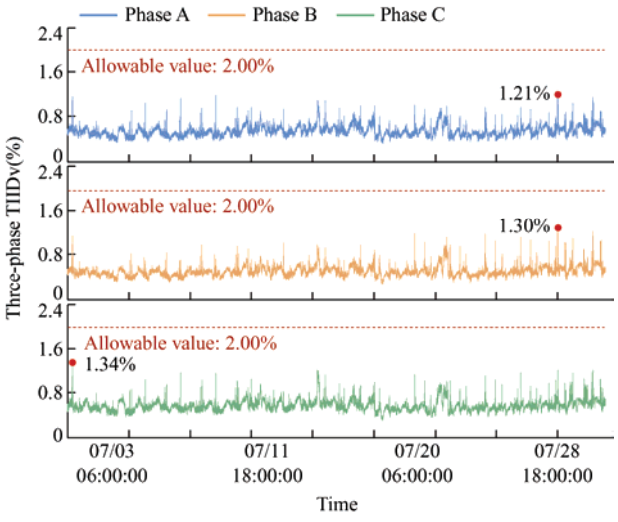

(b) Trend charts of three-phase THD_v at PCC

Fig. 9 Harmonic-suppression performance

Tab. 3 Measured THD_v values of the 110-kV bus

THDv	Phase A	Phase B	Phase C
95% probability value (%)	0.74	0.69	0.76
Allowable value (%)		2.00	

Tab. 4 Measured harmonic currents of the 110-kV bus

Harmonic order	95% probability value /A			Allowable value /A	
	Phase A	Phase B	Phase C		
5	4.61	3.93	3.79	12.80	Qualified
7	1.79	1.92	2.03	9.07	Qualified
11	0.69	0.64	0.58	5.73	Qualified
13	0.55	0.47	0.71	4.93	Qualified

4.2 Power factor

Fig. 10 displays time plots of the grid-side power factor (PF) when the wind-generated power is 4.53 MW and 11.29 MW, respectively. From Fig. 10, it can be seen that the average PFs are larger than 0.99 at both low and high power levels, and the minimum PFs in those conditions are larger than 0.95, indicating that the proposed system has a good reactive power compensation ability that meets the PF requirement.

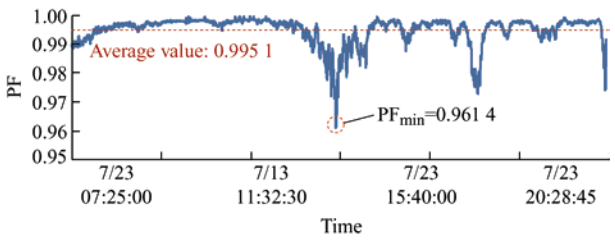

(a) S=4.53 MW

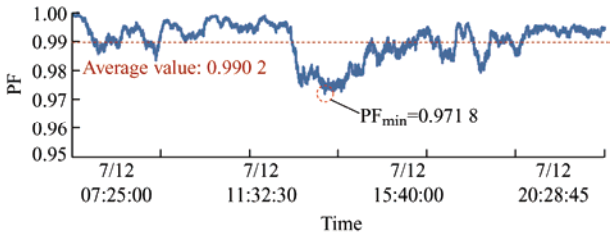

(b) S=11.29 MW

Fig. 10 Time plots of power factor at PCC

4.3 Voltage fluctuation and flicker

Voltage fluctuation refers to the ratio of the voltage RMS change to its normal value. A time plot for the voltage fluctuation is shown in Fig. 11, corresponding to the time interval in which the reactive power

fluctuates dramatically, and was adopted in our investigation. As shown in Fig. 11, the peak value of the voltage fluctuation at the PCC was 1.265%, which is lower than the limit of 1.50%.

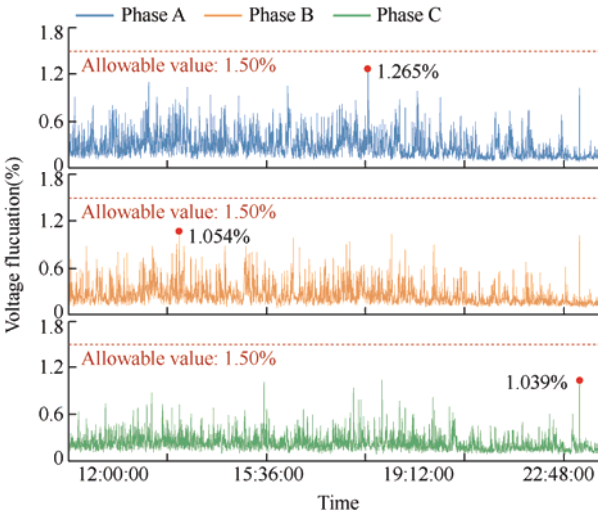

Fig. 11 Time plots of voltage fluctuation at PCC

The voltage flicker limits for each voltage level of the wind farm are listed in Tab. 5 (note: the LV, MV, and HV buses of the discussed system are shown in Fig. 2). The voltage flicker time plot waveform at the PCC of the entire measurement period is presented in Fig. 12, in which the short-time flicker is indicated by P_{st}, while the long-time flicker is P_{lt}. As shown in Fig. 12, the maximum values of P_{st} and P_{lt} are 0.532 and 0.234, respectively, and both are within the limits.

Tab. 5 Flicker limits

System voltage level	LV	MV	HV
P_{st}	1.0	0.9	0.8
P_{lt}	0.8	0.7	0.6

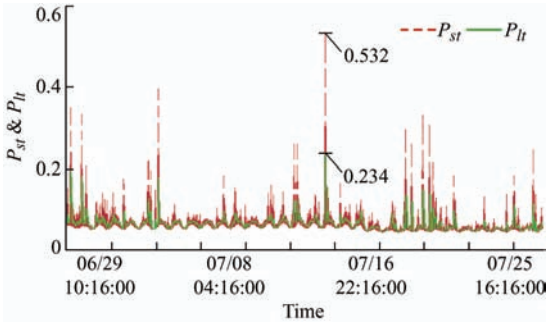

Fig. 12 Time plot of voltage flicker at PCC

Both Figs. 11 and 12 show that the combination of SVG and FTPF in the proposed IFT system can handle the dynamic voltage variation of the wind farm to address the voltage security issue economically.

5 Conclusions

A novel IFT-based grid-connected wind power scheme was proposed in this study for harmonic, resonance, reactive power, and voltage regulation. Its topology, mathematical model, harmonics, resonance filtering/damping mechanism, and performance have been discussed in detail. Recorded data from a real 50-MW IFT-based wind farm grid-connection system validated the feasibility of the proposed system. The conclusions drawn are summarized as follows.

(1) The proposed scheme has good suppression ability to block harmonic penetration from both the load and grid sides in a wind farm grid-connection system, and the harmonic content can meet the standard from the measured data of a real wind farm.

(2) The proposed scheme has the potential to suppress possible resonances arising from parameter disturbances in wind power grid-connection system applications.

(3) The combination of SVG and FTPF connected in the filtering winding of the IFT, as a self-adjusted reactive power source, can handle the PF, voltage fluctuation, and flicker in a wind farm grid-connection system with high cost efficiency.

The proposed system has been applied in practice; all the power quality indicators meet the standards of China, and its feasibility was verified.

References

[1] M R Islam, S Mekhilef, R Saidur. Progress and recent trends of wind energy technology. *Renewable and Sustainable Energy Reviews*, 2013, 12(5): 456-468.

[2] G F Gontijo, T C Tricarico, B W França, et al. Robust model predictive rotor current control of a DFIG connected to a distorted and unbalanced grid driven by a direct matrix converter. *IEEE Transactions on Sustainable Energy*, 2019, 10(3): 1380-1392.

[3] J C Y Hui, A Bakhshai, P K Jain. An energy management scheme with power limit capability and adaptive maximum power point tracking for small standalone PMSG wind energy systems. *IEEE Transactions on Power Electronics*, 2016, 31(7): 4861-4875.

[4] E Gatavi, A Hellany, M Nagrial, et al. An integrated reactive power control strategy for improving low voltage ride-through capability. *Chinese Journal of Electrical Engineering*, 2019, 5(4): 1-14.

[5] H Chen, D Xu, X Deng. Control for power converter of small-scale switched reluctance wind power generator. *IEEE Transactions on Industrial Electronics*, 2021, 68(4): 3148-3158.

[6] J Lin, Y Li, S Hu, et al. Resonance mechanism analysis of large-scale photovoltaic power plant. *Chinese Journal of Electrical Engineering*, 2021, 7(1): 47-54.

[7] Z H Rather, Z Chen, P Thøgersen, et al. Dynamic reactive power compensation of large-scale wind integrated power system. *IEEE Transactions on Power System*, 2015, 30(5): 2516-2526.

[8] E Guest, K H Jensen, T W Rasmussen. Mitigation of harmonic voltage amplification in offshore wind power plants by wind turbines with embedded active filters. *IEEE Transactions on Sustainable Energy*, 2020, 11(2): 785-794.

[9] K Hasan, K Rauma, A Luna, et al. Harmonic compensation analysis in offshore wind power plant using hybrid filters. *IEEE Transactions on Industry Applications*, 2014, 50(3): 2050-2060.

[10] Y Li, Y Peng, F Liu, et al. A controllably inductive filtering method with transformer-integrated linear reactor for power quality improvement of shipboard power system. *IEEE Transactions on Power Delivery*, 2017, 32(4): 1817-1827.

[11] Y Li, L Luo, C Rehtanz, et al. An industrial DC power supply system based on an inductive filtering method. *IEEE Transactions on Industrial Electronics*, 2012, 59(2): 714-722.

[12] Y Li, Q Liu, S Hu, et al. A virtual impedance comprehensive control strategy for the controllably inductive power filtering system. *IEEE Transactions on Power Electronics*, 2017, 32(2): 920-926.

[13] Q Liu, Y Li, S Hu, et al. Power quality improvement using controllable inductive power filtering method for industrial DC supply system. *Control Engineering Practice*, 2019, 83: 1-10.

[14] A K Pathak, M P Sharma, M Bundele. A critical review of voltage and reactive power management of wind farms. *Renewable and Sustainable Energy Reviews*, 2015, 51: 460-471.

[15] M Thompson, T Martini, N Seeley. Volt/VAR control for wind generation. 2012 *IEEE PES Transmission and Distribution Conference and Exposition,* 2012: 1-5.

[16] V B Virulkar, G V Gotmare. Sub-synchronous resonance in series compensated wind farm: A review. *Renewable and Sustainable Energy Reviews*, 2016, 55: 1010-1029.

[17] L Wang, C Chang, B Kuan, et al. Stability improvement of a two-area power system connected with an integrated onshore and offshore wind farm using a STATCOM. *IEEE Transactions on Industry Applications*, 2017, 53(2): 867-877.

[18] Y Li, L Luo, Z Zhang, et al. A DC power supply system developed with inductive filtering method. *Proceedings of the CSEE*, 2010, 30(22): 107-112.

[19] C Liang, Y Li, L Luo, et al. An integrated harmonic-filtering transformer for low voltage distribution systems. *IEEE Transaction on Magnetics*, 2015, 51(11): 1-4.

[20] Q Liu, Y Li, S Hu, et al. A transformer integrated filtering system for power quality improvement of industrial DC supply system. *IEEE Transactions on Industrial Electronics*, 2020, 67(5): 3329-3339.

[21] S B Vasyutinsky. Problems of theory and design of transformers. Translated by L Cui, E Du. Beijing: China Machine Press, 1983.

[22] F Lin, S Zuo, W Deng, et al. Modeling and analysis of electromagnetic force, vibration, and noise in permanent-magnet synchronous motor considering current harmonics. *IEEE Transactions on Industrial Electronics*, 2016, 63(12): 7455-7466.

[23] S Hu, Z Zhang, Y Chen, et al. A new integrated hybrid power quality control system for electrical railway. *IEEE Transactions on Industrial Electronics,* 2015, 62(10): 6222-6232.

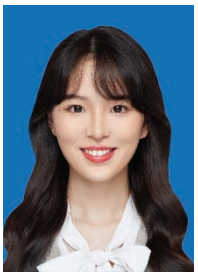

Juan Ni was born in Hengyang, Hunan, China, in 1998. She received the B.S. degree in Electrical Engineering from China University of Mining and Technology, Jiangsu, China, in 2019. She is currently working toward the M.S. degree in Electrical Engineering at the College of Electrical and Information Engineering, Hunan University, Changsha, China. Her research interest is electric power optimization and control.

Sijia Hu (S'14-M'16) was born in Hunan, China, in 1987. He received the B.S. and Ph.D. degrees in Electrical Engineering (and Automation) from Hunan University of Science and Technology, Xiangtan, China, and Hunan University (HNU), Changsha, China, in 2010 and 2015, respectively.

From May 2016 to Dec. 2019, and from Feb. 2017 to Dec. 2019, he was an Assistant Professor of Electrical Engineering with HNU, and a Research Fellow in the Institute of Power and Energy System in The University of Queensland (UQ), Bris-bane, Australia, respectively. Since January 2020, he is an Associate Professor of Electrical Engineering with HNU. His recent research interests include modeling, monitoring and energy management of railway power system, situation awareness and active control of distribution power system, optimal

design and control of converters.

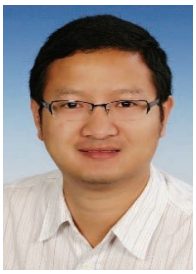

Yong Li (S'09-M'12-SM'14) was born in Henan, China, in 1982. He received the B.S. and Ph.D. degrees in 2004 and 2011, respectively, from the College of Electrical and Information Engineering, Hunan University, Changsha, China. Since 2009, he worked as a Research Associate at the Institute of Energy Systems, Energy Efficiency, and Energy Economics (IE3), TUDortmund University, Dortmund, Germany, where he received the second Ph.D. degree in June 2012. After then, he was a Research Fellow with The University of Queensland, Brisbane, Australia. Since 2014, he is a Full Professor of Electrical Engineering with Hunan University. His current research interests include power system stability analysis and control, ac/dc energy conversion systems and equipment, analysis and control of power quality, and HVDC and FACTS technologies.

Jinjie Lin was born in Fuzhou, Fujian, China, in 1995. He received the B.S. degree from Hunan University, Hunan, China, in 2018 and the M.E. degree in Electrical Engineering in 2020 from Hunan University, Changsha, China, where he is currently working toward the Ph.D. degree in Electrical Engineering from the College of Electrical and Information Engineering. His research interest is electric power optimization and control.

Qianyi Liu (S'16-M'21) was born in Sichuan, China, in 1992. He received the B.S. degree in Electrical Engineering and Its Automation (Railway Electrification) from the Department of Electrical Engineering, Southwest Jiaotong University in 2014, and received the M.E. and Ph.D. degrees in Electrical Engineering from the College of Electrical and Information Engineering, Hunan University in 2017 and 2020. From 2019 to 2020, he was a visiting Ph.D. student at the Institute of Energy Systems, Energy Efficiency, and Energy Economics (IE3), TU Dortmund University, Dortmund, Germany. Since 2021, he has been a Lecturer of Electrical Engineering with School of Automation, Central South University, Changsha, China. His research interest is electric power optimization and control.

Peiyao Liu was born in Yiyang, Hunan, China, in 1998. She received the B.S. degree in Electrical Engineering from Hohai University, Jiangsu, China, in 2020. She is currently pursuing the M.S degree with the College of Electrical and Information Engineering, Hunan University, Changsha, China. Her research interests include electric power analyses and control.

Lihong Dong was born in Yiyang, Hunan, China, in 1997. He received the B.S. degree in Electric Engineering and Automation from Hunan University, Changsha, China, in 2019. He is currently pursuing the M.S degree with the College of Electrical and Information Engineering, Hunan University, Changsha, China. His current research interests are power quality analyses and high power electroacoustic transducer.